RESEARCH ARTICLE

WILEY

# Brain connectivity markers for the identification of effective contacts in subthalamic nucleus deep brain stimulation

Hai Lin[1,2,3]   |   Peng Na[1,2,3]   |   Doudou Zhang[1,3]   |   Jiali Liu[1,3]   |   Xiaodong Cai[1,3]   |   Weiping Li[1,2,3]

[1]Department of Neurosurgery, Shenzhen Second People's Hospital, First Affiliated Hospital of Shenzhen University, Shenzhen, Guangdong, China

[2]Shenzhen Key Laboratory of Neurosurgery, Shenzhen Second People's Hospital, First Affiliated Hospital of Shenzhen University, Shenzhen, Guangdong, China

[3]Shenzhen University School of Medicine, Shenzhen, Guangdong, China

**Correspondence**
Weiping Li, Brain Centre, Shenzhen Key Laboratory of Neurosurgery, Shenzhen Second People's Hospital, the First Affiliated Hospital of Shenzhen University, Shenzhen University School of Medicine, 3002# Sungang West Road, Futian District, Shenzhen 518035, China.
Email: wpli@szu.edu.cn

## Abstract

The clinical benefit of deep brain stimulation (DBS) for Parkinson's disease (PD) is relevant to the tracts adjacent to the stimulation site, but it remains unclear what connectivity pattern is associated with effective DBS. The aim of this study was to identify clinically effective electrode contacts on the basis of brain connectivity markers derived from diffusion tensor tractography. We reviewed 77 PD patients who underwent bilateral subthalamic nucleus DBS surgery. The patients were assigned into the training ($n = 58$) and validation ($n = 19$) groups. According to the therapeutic window size, all contacts were classified into effective and ineffective groups. The whole-brain connectivity of each contact's volume of tissue activated was estimated using tractography with preoperative diffusion tensor data. Extracted connectivity features were put into an all-relevant feature selection procedure within cross-validation loops, to identify features with significant discriminative power for contact classification. A total of 616 contacts on 154 DBS leads were discriminated, with 388 and 228 contacts being classified as effective and ineffective ones, respectively. After the feature selection, the connectivity of contacts with the thalamus, pallidum, hippocampus, primary motor area, supplementary motor area and superior frontal gyrus was identified to significantly contribute to contact classification. Based on these relevant features, the random forest model constructed from the training group achieved an accuracy of 84.9% in the validation group, to discriminate effective contacts from the ineffective. Our findings advanced the understanding of the specific brain connectivity patterns associated with clinical effective electrode contacts, which potentially guided postoperative DBS programming.

**KEYWORDS**

brain connectivity, DBS programming, deep brain stimulation, Parkinson's disease, subthalamic nucleus

# 1 | INTRODUCTION

Deep brain stimulation (DBS) is currently a well-established medical therapy for movement disorders such as Parkinson's disease (PD), essential tremor, and dystonia, and is being explored for a variety of other neurological and psychiatric diseases (Miocinovic, Somayajula, Chitnis, & Vitek, 2013). In PD, two main DBS targets are the subthalamic nucleus (STN) and the globus pallidus pars interna (Odekerken et al., 2013; Shukla & Okun, 2014), which are both subcortical nuclei in gray matter structures. There are some electrophysiological evidences indicating that DBS actually excites neuronal fibers, but inhibits cell bodies (McIntyre, Grill, Sherman, & Thakor, 2004; McIntyre & Hahn, 2010). Therefore, the white matter tracts adjacent to the stimulation site should be related to the DBS therapeutic effects.

Diffusion tensor imaging (DTI) is a MRI technique that allows to non-invasively map white matter tractography in the brain, by measuring the diffusion of water molecules through tissue (Jones, 2008). Within the last few years, this modality has been applied for the preoperative target localization of DBS surgery, such as the visualization of the dentato-rubro-thalamic tract optimizing target definition for tremor control (Coenen et al., 2014) and the four-bundle white matter blueprint for subcallosal cingulate DBS targeting in treatment-resistant depression (Riva-Posse et al., 2018). As to the STN-DBS for PD patients, STN can be functionally divided into motor (dorsolateral), limbic (medial), and associative (ventromedial) sub-regions, based on the topography of cortico-subthalamic projections (Lambert et al., 2012). The motor part of STN is known to receive motor input and be the stimulation site that obtained the best motor improvement (Johnsen, Sunde, Mogensen, & Østergaard, 2010; Wodarg et al., 2012). A patient-specific dissection of the STN subdivisions could be achieved using fiber tracking from diffusion-weighted images, which might facilitate individualized surgical planning (Plantinga et al., 2018). Akram et al. (2017) further found that the optimal DBS site for PD symptoms of tremor, bradykinesia, and rigidity appears to correspond to different areas in the motor STN. Furthermore, DBS-cortical connectivity, along the hyperdirect pathways (Nambu, Tokuno, & Takada, 2002; Williams et al., 2002) to primary motor area (M1), supplementary motor area (SMA), and prefrontal cortex, is predictive of maximum improvement for different motor symptoms.

White matter tractography can not only optimize preoperative DBS targeting, but also provide reference for contact selection in postoperative DBS programming. The monopolar review, evaluating motor improvement and side effects for each contact, is currently the standard procedure during programming (Volkmann, Herzog, Kopper, & Deuschl, 2002). As more complex electrodes with multiple contacts, such as directional leads with multiple independent current controls, are applied and replace the conventional quadripolar electrode in the near future (Kühn & Volkmann, 2017; Pollo et al., 2014), DBS programming will become much more time-consuming. In a recent study, the distance of active contacts to the hyperdirect pathway was found to be related to the improvement of motor symptoms after DBS (Chen et al., 2018). Moreover, Zhang et al. (2019) found that the number of tracts through the volumes of tissue activated (VTAs) of contacts and M1/SMA showed significant differences between clinical optimal and nonoptimal contacts. By the whole-brain tractography rather than limited to the specific tracts, areas that most frequently connected to clinically effective contacts included the thalamus, substantia nigra, brainstem, and superior frontal gyrus (SFG), and the strength of connectivity to the thalamus and SFG were positively associated with clinical effectiveness, which were demonstrated in a DTI study (Vanegas-Arroyave et al., 2016). However, these discriminative factors were found in PD patients from a relatively small cohort. With sufficient number of patients, multi-factor models can be constructed to distinguish between effective and ineffective contacts, which potentially help contact selection in DBS programming.

In this study, we reviewed PD patients who underwent bilateral STN-DBS surgery and performed preoperative DTI-based tractography to obtain the brain connectivity patterns of all contacts. We then identified relevant connectivity features with significant discriminative power for contact classification under an all-relevant feature selection procedure and constructed a random forest model to discriminate clinically effective contacts from the ineffective.

# 2 | MATERIALS AND METHODS

## 2.1 | Patients

77 idiopathic PD patients who underwent bilateral STN-DBS surgery at the Department of Functional Neurosurgery, Shenzhen Second People's Hospital between January 2017 and September 2019 were consecutively recruited. All patients met UK Brain Bank criteria for idiopathic PD (Hughes, Daniel, Kilford, & Lees, 1992) and obtained an improvement rate > 25% on the Unified Parkinson's Disease Rating Scale-part III (UPDRS-III) in the L-DOPA challenge test, assessed by a multi-disciplinary team of specialized movement disorders neurologists and functional neurosurgeons. In addition, patients underwent neuropsychological evaluation and structural MRI scanning to rule out dementia and significant brain atrophy, respectively. The patients were assigned to the training ($n$ = 58) and validation ($n$ = 19) groups. This study was approved by the local ethics committee of our hospital for human research. All participants were fully informed about the purpose and procedure of the study, and provided written informed consent before enrollment.

## 2.2 | Preoperative MR images

Preoperative MRI scanning was performed on a 3T system (Prisma, Siemens, Erlangen, Germany) using a 32-channel head coil. The protocol included high-resolution T1- and T2-weighted MR images, along with a diffusion-weighted imaging acquisition (echo-planar imaging, 60 weighted directions, and 2 b0 images, $b$ = 1,000 s/mm$^2$, TR/TE = 8300/80 ms, resolution $2 \times 2 \times 2$ mm$^3$).

## 2.3 | Surgical procedure

The surgeries were performed in a locally anesthetic condition, using Leksell Stereotactic System (Elekta AB, Stockholm, Sweden). Two DBS electrodes (PINS L301, Beijing, China) targeting the STN were implanted in both sides of brain. Lead placement was the most important process for the operation. The place to obtain the best clinical efforts was evaluated and confirmed by single unit microelectrode recording and stimulation on wake patients during the operation. The dorsolateral portion of the nucleus is known to receive motor input and be the stimulation site that obtained the best motor improvement. The target coordinates were defined by a composite method combining Indirect Targeting and Red nucleus-based Targeting (Toda et al., 2009). After validation of lead placement by microelectrode recording and stimulation, the electrodes were connected to the pulse generator (G102R, PINS, Beijing, China), which was implanted subcutaneously in the left subclavicular region.

## 2.4 | Postoperative CT scanning and DBS programming

A 1 mm head CT scanning was performed right before DBS programming, using a 40-row spiral system (Somatom definition, AS; Siemens, Erlangen, Germany). One month after DBS surgery, an experienced neurologist implemented DBS programming on all patients (more than 12 hours after the withdrawal of their dopaminergic medications in a clinically defined "off-state") with the monopolar review strategy. Monopolar screening was performed for each of the four contacts on each lead. The initial DBS parameters were as follows: pulse width of 60 ms, frequency of 130 Hz, and voltage amplitude of 0.5 V. The amplitude of stimulation voltage was gradually increased at a step of 0.5 V to determine each contact's therapeutic window. The minimum voltage where motor improvement first appeared for each patient's predominant parkinsonian symptoms (tremor, rigidity or bradykinesia)

was defined as the window entry. And the maximum voltage where side effects (such as facial pulling, dysarthria, diplopia, and paresthesia) occurred or 6.0 V if there were no side effects was defined as the window exit. The window size was calculated by subtracting the window entry from the window exit.
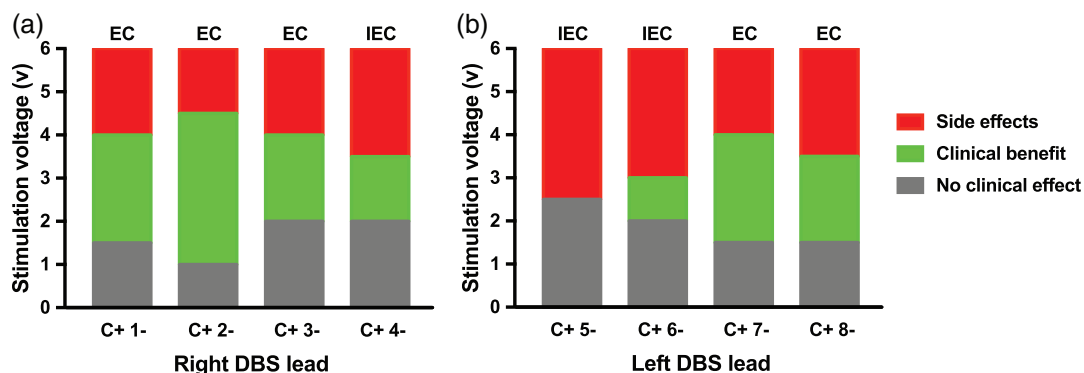
The contacts with the therapeutic window size ≥2 V were classified as clinically effective contacts and the others as ineffective ones. An example of contact classification outcome in a PD patient is displayed in Figure 1. The stimulating contact was determined for each lead to obtain the largest therapeutic window and the best motor improvement (Volkmann, Moro, & Pahwa, 2006). DBS lead therapeutic impedances were recorded for the stimulating contacts with the final setting.

## 2.5 | DBS electrode localization and VTA estimation

DBS electrodes were localized using the toolbox of Lead-DBS (http://www.lead-dbs.org) in Matlab (MathWorks, Natick, Massachusetts). The main steps included linear coregistration between postoperative CT and preoperative MRI, normalization to the standardized Montreal Neurological Institute (MNI) space, pre-reconstruction of electrode trajectories and manual correction of electrode localization (Horn & Kühn, 2015). After localization, the VTA was estimated for each contact as previous described in Horn et al. (2017), using the window entry voltage as the stimulation voltage (Vanegas-Arroyave et al., 2016; Figure 2a).

## 2.6 | Image preprocessing

Diffusion weighted imaging data were analyzed using FSL toolbox. Motion and eddy current distortions were corrected using the "eddy" script. A brain mask of the non-diffusion-weighted image was created using the BET in FSL. Diffusion tensors were calculated using the



**FIGURE 1** An example of contact classification outcome in a PD patient. During the initial programming session, the contacts with the therapeutic window size ≥2 V were classified as clinically effective contacts (EC) and the others were classified as ineffective contacts (IEC). Gray = no clinical benefit was observed; green = the therapeutic window between window entry and window exit voltages; red = side effects were observed. PD, Parkinson's disease

"dtifit" script, and the resulting fractional anisotropy (FA) images were linearly co-registered in native space to their corresponding T1-weighted images. Preoperative structural images were then non-linearly registered to the standard MNI space (the ICBM152 template). The automated anatomical labeling (AAL) atlas in the standard space was used to inversely warp images back to individual native space by applying the inverse transformation of the above two steps. This atlas contained 116 gray matter regions of interest. The corresponding regions in both hemispheres, such as the right and left thalamus, were merged. In addition, four specific sub-nuclei including the red nucleus, substantia nigra, STN, and hypothalamus were added to the segmented brain, which resulted in a total of 66 sub-regions.

## 2.7 | Tractography

Deterministic tractography was performed in subject-specific native space using the fiber assignment by continuous tracking (FACT) algorithm in Diffusion Toolkit (http://www.trackvis.org/dtk/). A streamline was started from each seed (eight seeds per voxel) and terminated when it reached a voxel with an FA value lower than 0.2, or when the streamline exceeded the brain mask, or when the trajectory of the streamline made a turn sharper than $45°$.

## 2.8 | Feature extraction

For each contact, we estimated the strength of connectivity between the corresponding VTA and 66 segmented regions. Averaged FA values, calculated from all the streamlines through both the VTA and segmented regions, defined the connectivity strength, which resulted in 66 connectivity features (Figure 3). Additionally, connectivity analysis employed streamline count instead of averaged FA value for the measurement. To normalize for differences in voltage and VTA volume, we defined the connectivity strength as the fraction of the number of the streamlines through both the VTA and segmented regions to the total number of the streamlines through the VTA (streamline fraction).

## 2.9 | Feature selection and model construction

To identify features with significant discriminative power for contact classification, all connectivity features were put into an all-relevant feature selection procedure within cross-validation loops using the random forest algorithm (Figure S1), as described in a previous study (Sun et al., 2017). All electrode contacts in the training group (58 patients) were divided into two groups: clinically effective and ineffective contacts. The selection procedure was embedded in a repeated 10-fold cross-validation framework (repeated 100 times) to
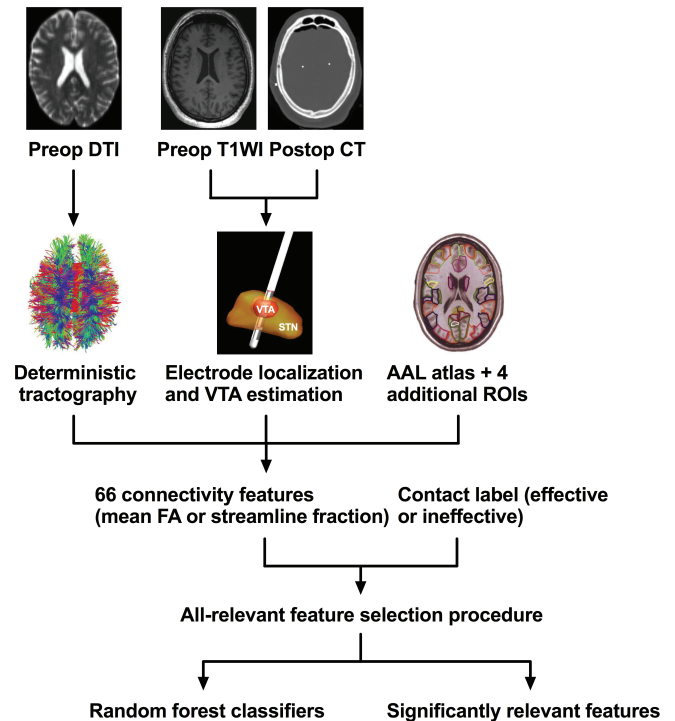


**FIGURE 3** Flow diagram representing steps for feature extraction and selection. AAL, automated anatomical labeling; Preop DTI, preoperative diffusion tensor imaging; FA, fractional anisotropy; Preop T1WI, preoperative T1-weighted image; Postop CT, postoperative computed tomography; ROIs, regions of interest; STN, subthalamic nucleus; VTA, volume of tissue activated
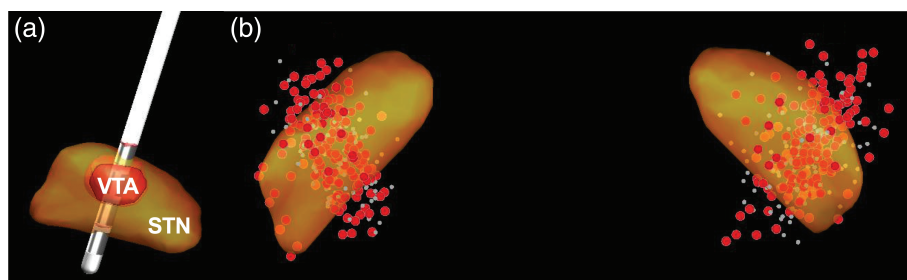


**FIGURE 2** The VTA estimation and DBS electrode localization. (a) The volume of tissue activated (VTA) was estimated for each electrode contact, using the window entry voltage as the stimulation voltage. (b) 154 DBS electrodes were located in standardized MNI space together with the subthalamic nucleus (STN), according to the DISTAL atlas. A total of 616 contacts were discriminated, with 388 and 228 contacts being classified as clinically effective (red dots) and ineffective (gray dots) contacts, respectively

obtain unbiased estimates of classification error. For each iteration, a random forest classifiers was constructed from the training set using the randomForest package (Svetnik et al., 2003) in Matlab (MathWorks, Natick, MA). The performance of the classifier was evaluated in the validation set. Among all iterations, different subsets of features were selected on the basis of different folds. The selection frequency of each feature was defined as the number of iterations in which the feature was selected divided by the total number of iterations. Features with significantly higher selection frequency than random values defined by permutation test (permuted 1,000 times; Sun et al., 2017) were identified as effectiveness-related selections, with $p$ value <.05 after false discovery rate (FDR) correction for multiple comparisons (Benjamini & Hochberg, 1995). On basis of identified features, the last random forest model was built from the training group (58 patients) and was further evaluated in the validation group (19 patients).

## 3 | RESULTS

### 3.1 | Clinical outcomes

The demographic characteristics and clinical information of all patients were listed in Table 1. There were no significant differences in age, sex, PD duration, levodopa equivalent daily dose (LEDD) or UPDRS-III scores between training and validation groups (two-tailed $t$-tests, all

$p$ values >.05). One month after the DBS surgery, patients obtained a significant improvement of the UPDRS-III score (28.8 ± 9.0; preoperative UPDRS-III score when medication off, 50.7 ± 14.9; postoperative UPDRS-III score when medication off, 21.9 ± 6.9; $p$ < .001 in a paired $t$-test).

154 DBS electrodes were located in standardized MNI space together with the STN (Figure 2b), according to the DISTAL atlas (Ewert et al., 2018). A total of 616 contacts were discriminated, with 388 and 228 contacts being classified as clinically effective and ineffective contacts, respectively. MNI coordinates of effective contacts' centers in the right and left hemispheres were $x = 12.7 ± 1.5$, $y = −13.5 ± 2.2$, $z = −7.9 ± 2.4$ and $x = −11.8 ± 1.2$, $y = −13.8 ± 2.3$, $z = −7.6 ± 2.5$ (mean ± $SD$), respectively. The coordinates of ineffective contacts' centers in both hemispheres were $x = 13.3 ± 1.8$, $y = −12.9 ± 2.1$, $z = −7.6 ± 3.0$ and $x = −12.3 ± 1.4$, $y = −13.1 ± 1.9$, $z = −7.4 ± 2.8$, respectively. Effective and ineffective contacts showed no differences in the MNI coordinates, using Kolmogorov–Smirnov tests (all $p$ values >.05, after FDR correction; Table 2).

### 3.2 | The performance of random forest classifiers

In constructing and evaluating the classifiers to discriminate effective contacts from the ineffective, we repeated 100 times of 10-fold cross validation, which resulted in a total of 1,000 training–testing cycles.

**TABLE 1** The demographic and clinical information of all patients

| | Total ($n = 77$) | Training ($n = 58$) | Validation ($n = 19$) | $p$ value[a] |
|---|---|---|---|---|
| Age (years) | 59.8 ± 10.5 | 59.6 ± 10.0 | 60.4 ± 10.7 | .78 |
| Sex (M/FM) | 45/32 | 33/25 | 12/7 | .63[b] |
| PD duration (years) | 8.3 ± 2.6 | 8.4 ± 2.4 | 7.9 ± 2.5 | .45 |
| LEDD | 1,050.7 ± 477.2 | 1,064.5 ± 486.3 | 1,008.4 ± 459.1 | .66 |
| Preop UPDRS-III | 50.7 ± 14.9 | 52.0 ± 15.1 | 46.8 ± 14.2 | .18 |
| Postop UPDRS-III | 21.9 ± 6.9 | 22.6 ± 7.3 | 19.8 ± 5.9 | .12 |
| UPDRS-III improvement | 28.8 ± 9.0 (56.8%) | 29.4 ± 9.2 (56.5%) | 27.0 ± 8.7 (57.7%) | .32 |

*Note:* Values are represented as the mean ± SD, except for the gender distribution.
Abbreviations: FM, female; LEDD, levodopa equivalent daily dose; M, male; Preop, preoperative; Postop, postoperative; UPDRS-III, Unified Parkinson's Disease Rating Scale part III.
[a]Unless otherwise indicated, $p$ values were calculated with two-tailed $t$-tests between training and validation groups.
[b]$p$ Value was obtained using a chi-squared test between training and validation groups.

**TABLE 2** The MNI coordinates of effective and ineffective contacts' centers in right and left hemispheres

| | Right hemisphere | | | Left hemisphere | | |
|---|---|---|---|---|---|---|
| | Effective contacts | Ineffective contacts | $p$ Value[a] | Effective contacts | Ineffective contacts | $p$ Value[a] |
| Number | 204 | 104 | | 184 | 124 | |
| MNI_X | 12.7 ± 1.5 | 13.3 ± 1.8 | .10 | −11.8 ± 1.2 | −12.3 ± 1.4 | .14 |
| MNI_Y | −13.5 ± 2.2 | −12.9 ± 2.1 | .10 | −13.8 ± 2.3 | −13.1 ± 1.9 | .075 |
| MNI_Z | −7.9 ± 2.4 | −7.6 ± 3.0 | .26 | −7.6 ± 2.5 | −7.4 ± 2.8 | .32 |

*Note:* MNI coordinates are represented as the mean ± SD.
Abbreviations: MNI_X, Coordinate X in MNI space; MNI_Y, Coordinate Y in MNI space; MNI_Z, Coordinate Z in MNI space.
[a]Kolmogorov–Smirnov test and FDR correction were performed.

The accuracy and Cohen's kappa coefficient of the random forest classifiers were 87.2 ± 4.1% and 0.63 ± 0.19, with features from the all-relevant feature selection process. The corresponding sensitivity and specificity were 90.5 ± 5.6% and 85.1 ± 6.8%, respectively.

## 3.3 | Significantly relevant features

After the feature selection was embedded into the 10-fold cross-validation procedure, a total of 1,000 feature subsets were created for each random forest classifier. In the construction of the classifier discriminating between effective and ineffective contacts, the mean number of features in each subset was 7.6 (range from 5 to 10; 7.6–15.2% of all 66 features). Six connectivity features were identified to be significantly relevant, with their selection frequencies being significantly higher than random values derived from the permutation test (Table 3). These six features were the strength of connectivity to the thalamus, hippocampus, pallidum, M1, SMA, and SFG defined by the mean FA value. Moreover, These features of effective contacts were significantly larger than that of ineffective contacts, using Kolmogorov–Smirnov tests (all *p* values <.001, after FDR correction; Figure 4). That is to say, the stronger the connectivity of a contact with each of these six relevant brain regions was, the greater the probability of being an effective contact was.

When streamline fraction replaced mean FA to define the connectivity strength, similar results were obtained except that the connectivity to the pallidum was not relevant to contact classification.

**TABLE 3** Significantly relevant connectivity features to discriminate between effective and ineffective contacts

| Selection frequency (%)[a] | Feature description | Effective contacts | Ineffective contacts |
|---|---|---|---|
| 93.1 | Strength of connectivity between the VTA and thalamus | 0.54 ± 0.20 | 0.32 ± 0.18 |
| 91.8 | Strength of connectivity between the VTA and SMA | 0.27 ± 0.13 | 0.16 ± 0.10 |
| 91.2 | Strength of connectivity between the VTA and SFG | 0.31 ± 0.16 | 0.19 ± 0.11 |
| 88.5 | Strength of connectivity between the VTA and M1 | 0.25 ± 0.11 | 0.17 ± 0.09 |
| 84.4 | Strength of connectivity between the VTA and hippocampus | 0.31 ± 0.18 | 0.24 ± 0.14 |
| 80.6 | Strength of connectivity between the VTA and pallidum | 0.36 ± 0.22 | 0.28 ± 0.20 |

*Note:* The connectivity strength (mean ± *SD*) was defined by the averaged FA value.
Abbreviations: M1, primary motor area; SFG, superior frontal gyrus; SMA, supplementary motor area; VTA, volume of tissue activated.
[a]Defined as the number of iterations in which the feature was selected divided by the total number of iterations performed.
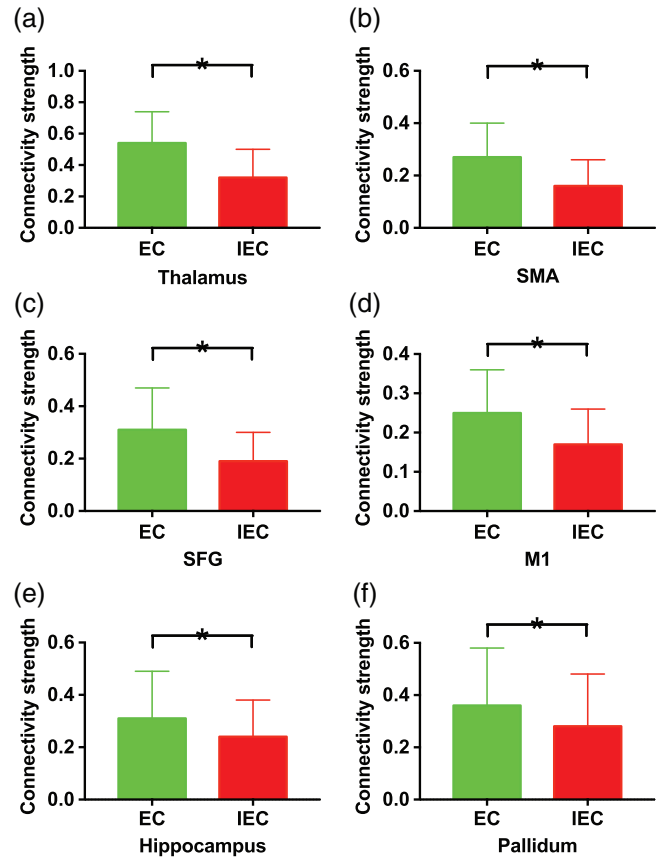


**FIGURE 4** The comparisons of six connectivity features between effective and ineffective contacts. These features were the strength of connectivity to the (a) thalamus, (b) SMA, (c) SFG, (d) M1, (e) hippocampus and (f) pallidum, defined by the mean FA value. They all showed significant differences using Kolmogorov–Smirnov tests (all *p* values <.001, after FDR correction). The symbol (∗) indicates being significant. EC, effective contacts; FA, fractional anisotropy; IEC, ineffective contacts; M1, primary motor area; SFG, superior frontal gyrus; SMA, supplementary motor area

## 3.4 | Connectivity-based prediction of contacts' effectiveness

In the training group (58 patients), six connectivity features related to contacts' effectiveness were screened by the feature selection procedure. Based on these relevant features, the random forest model constructed from the training group achieved an accuracy of 84.9% in the validation group (19 patients), to discriminate effective contacts from the ineffective.

## 4 | DISCUSSION

In brief, our study provided an effective connectivity-based model that discriminated between clinically effective and ineffective electrode contacts in PD patients treated with STN-DBS. Brain connectivity markers of effective contacts, including the connectivity to the

thalamus, hippocampus, pallidum, M1, SMA, and SFG, were identified through the all-relevant feature selection procedure.

In this study, we investigated the whole-brain connectivity to the stimulation site based on diffusion-weighted MR images and established an analytic framework through machine learning methods, to characterize the specific connectivity patterns of effective DBS. Extracted features were put into an all-relevant feature selection procedure within cross-validation loops using the random forest algorithm. To train binary classifiers, the two-sample $t$-test is commonly used as the feature selection method. The $p$ value in a $t$-test indicates the consistency of difference between two groups rather than the magnitude of difference, which suggests that the two-sample $t$-test may be not optimal for feature selection. In comparison, the all-relevant feature selection screens out all features that provide information usable for classification and significantly contribute to group discrimination. Thus, the analytic framework can identify all features relevant to the contact selection and characterize the specific connectivity patterns of effective contacts.

The STN, a small lens-shaped nucleus in basal ganglia, connects with other basal ganglia and several cortical areas. The STN is surrounded by dense bundles of white matter fibers such as the subthalamopallidal and pallidothalamic fibers, which are parts of the indirect pathway for the motor circuitry of the basal ganglia. The indirect pathway exerts surround inhibition to facilitate an excitatory drive to muscles responsible for a given movement and suppress unwanted motor activity not relevant to the primary movement (Mehanna & Jankovic, 2013). PD is thought to be of great concern to over-activation of the indirect pathway (Mehanna & Lai, 2013). In our study, the connectivity of contacts with the thalamus and pallidum was found to be related to the therapeutic effects of STN-DBS in PD, which might be explained by the inhibitory effects of DBS and the subthalamopallidal and pallidothalamic fibers surrounding the STN. This result was consistent with the finding that the strength of connectivity to the thalamus was positively associated with clinical effectiveness of STN-DBS in a DTI study (Vanegas-Arroyave et al., 2016).

In addition to the indirect pathway, the descending fibers from Brodmann area 6 and M1 enter the STN in its dorsal aspect, constituting the motor component of the hyperdirect pathway (Haynes & Haber, 2013). This study reveals a stronger connectivity of effective contacts with the M1, SMA being located in the medial aspect of Brodmann area 6 and SFG containing the dorsal and anterior areas of Brodmann area 6, than that of ineffective contacts. Some previous studies investigating the association between brain connectivity and clinical outcome of DBS obtained similar results (Akram et al., 2017; Horn et al., 2017; Vanegas-Arroyave et al., 2016). Horn et al. (2017) found that the structural connectivity of the electrode to SMA positively correlated with clinical response of STN-DBS. Akram et al. (2017) revealed that DBS-cortical connectivity to M1, SMA, and prefrontal cortex was predictive of maximum improvement for different motor symptoms. These consistent findings further support the role of STN-based connectivity in the STN-DBS's mechanism of action for PD.

Although STN-DBS is an effective therapy for PD, the therapeutic effects still vary among PD patients and the corresponding precise mechanisms remain unclear. In this study, effective and ineffective contacts showed significant differences in the identified connectivity features extracted from tractography, but no differences in the MNI coordinates, which suggested that relevant white matter tracts near the STN might be more important than the same stimulation site for the DBS therapeutic effects in different PD patients. This was also supported by the electrophysiological finding that DBS decouples neuronal somatic and axonal activity—inhibiting cell bodies and simultaneously generating orthodromic and antidromic axonal action potentials (Johnson & McIntyre, 2008). Moreover, clinical studies started to use tractography for the preoperative target localization of DBS, such as the visualization of the dentato-rubro-thalamic tract optimizing target definition for tremor control (Coenen et al., 2014) and the four-bundle white matter blueprint for subcallosal cingulate DBS targeting in treatment-resistant depression (Riva-Posse et al., 2018). Therefore, our findings and related studies might advance our understanding of the neural substrates of the DBS therapeutic effects and provide the potential for personalized DBS therapy in PD.

Postoperative DBS programming consists of contact selection and parameter management (Volkmann et al., 2002). As more complex electrodes with multiple contacts, such as directional leads with multiple independent current controls, are applied and replace the conventional quadripolar electrode in the near future (Kühn & Volkmann, 2017; Pollo et al., 2014), DBS programming by the monopolar review strategy will become more time-consuming. Within the last few years, several studies explored the clinical value of neuroanatomical information about electrode contacts' locations based on postoperative structural MR images (Petersen et al., 2018; Zhang et al., 2019). Petersen et al. (2018) calculated contacts' locations by an automated electrode reconstruction and revealed that most contacts chosen to deliver stimulation were closest or second closest to the atlas-based STN target. Additionally, Zhang et al. (2019) found that the distances of contacts to the STN showed significant differences between clinical optimal and nonoptimal contacts. In this study, the strength of connectivity to the thalamus, pallidum, hippocampus, M1, SMA, and SFG showed significant differences between effective and ineffective contacts. More importantly, the connectivity-based model achieved the accuracy of 84.9% to discriminate effective contacts from the ineffective, which potentially guided clinicians to select effective contacts.

We acknowledge a few limitations to our study. First, the connectivity analysis was based on preoperative DTI data, rather than the postoperative. Thus, the corresponding results possibly change due to brain shift, cell death or other surgical effects. Second, UPDRS-III scores were evaluated only for the stimulating contacts, but not all contacts. So we defined the effectiveness of contacts according to the therapeutic window size, rather than the magnitude of motor improvement assessed by the UPDRS-III score. Lastly, the effectiveness of contacts was evaluated 1 month after DBS surgery. More follow-up clinical outcomes, including programming optimization, UPDRS-III scoring, and LEDD reduction, should be recorded and analyzed in future study.

# 5 | CONCLUSION

In this study, an effective model was constructed to discriminate clinical effective contacts from the ineffective, which potentially guided postoperative DBS programming. The connectivity of contacts with the thalamus, hippocampus, pallidum, M1, SMA, and SFG, significantly contributing to contact classification, could serve as the brain connectivity markers for the identification of effective contacts in STN-DBS.

## CONFLICT OF INTEREST

The authors declare that they have no competing interests.

## AUTHOR CONTRIBUTIONS

H.L., X.C., and W.L. conceived and designed the study. P.N., D.Z., and J.L. performed research. H.L. and P.N. analyzed the data. H.L. wrote and X.C. commented the manuscript.

## DATA AVAILABILITY STATEMENT

Data available on request due to privacy/ethical restrictions.

## ORCID

*Weiping Li* https://orcid.org/0000-0002-4391-3112

## REFERENCES

Akram, H., Sotiropoulos, S. N., Jbabdi, S., Georgiev, D., Mahlknecht, P., Hyam, J., ... Hariz, M. (2017). Subthalamic deep brain stimulation sweet spots and hyperdirect cortical connectivity in Parkinson's disease. *NeuroImage*, *158*, 332–345. https://doi.org/10.1016/j.neuroimage.2017.07.012

Benjamini, Y., & Hochberg, Y. (1995). Controlling the false discovery rate: A practical and powerful approach to multiple testing. *Journal of the Royal Statistical Society: Series B (Methodological)*, *57*(1), 289–300. https://doi.org/10.1111/j.2517-6161.1995.tb02031.x

Chen, Y., Ge, S., Li, Y., Li, N., Wang, J., Wang, X., ... Luo, T. (2018). Role of the cortico-subthalamic hyperdirect pathway in deep brain stimulation for the treatment of Parkinson disease: A diffusion tensor imaging study. *World Neurosurgery*, *114*, e1079–e1085. https://doi.org/10.1016/j.wneu.2018.03.149

Coenen, V. A., Allert, N., Paus, S., Kronenbürger, M., Urbach, H., & Mädler, B. (2014). Modulation of the cerebello-thalamo-cortical network in thalamic deep brain stimulation for tremor: A diffusion tensor imaging study. *Neurosurgery*, *75*(6), 657–670. https://doi.org/10.1227/NEU.0000000000000540

Ewert, S., Plettig, P., Li, N., Chakravarty, M. M., Collins, D. L., Herrington, T. M., ... Horn, A. (2018). Toward defining deep brain stimulation targets in MNI space: A subcortical atlas based on multimodal MRI, histology and structural connectivity. *NeuroImage*, *170*, 271–282. https://doi.org/10.1016/j.neuroimage.2017.05.015

Haynes, W. I., & Haber, S. N. (2013). The organization of prefrontal-subthalamic inputs in primates provides an anatomical substrate for both functional specificity and integration: Implications for basal ganglia models and deep brain stimulation. *Journal of Neuroscience*, *33*(11), 4804–4814. https://doi.org/10.1523/JNEUROSCI.4674-12.2013

Horn, A., & Kühn, A. A. (2015). Lead-DBS: A toolbox for deep brain stimulation electrode localizations and visualizations. *NeuroImage*, *107*, 127–135. https://doi.org/10.1016/j.neuroimage.2014.12.002

Horn, A., Reich, M., Vorwerk, J., Li, N., Wenzel, G., Fang, Q., ... Kühn, A. A. (2017). Connectivity predicts deep brain stimulation outcome in parkinson disease. *Annals of Neurology*, *82*(1), 67–78. https://doi.org/10.1002/ana.24974

Hughes, A. J., Daniel, S. E., Kilford, L., & Lees, A. J. (1992). Accuracy of clinical diagnosis of idiopathic Parkinson's disease: A clinico-pathological study of 100 cases. *Journal of Neurology, Neurosurgery & Psychiatry*, *55*(3), 181–184. https://doi.org/10.1136/jnnp.55.3.181

Johnsen, E. L., Sunde, N., Mogensen, P. H., & Østergaard, K. (2010). MRI verified STN stimulation site–gait improvement and clinical outcome. *European Journal of Neurology*, *17*(5), 746–753. https://doi.org/10.1111/j.1468-1331.2010.02962.x

Johnson, M. D., & McIntyre, C. C. (2008). Quantifying the neural elements activated and inhibited by globus pallidus deep brain stimulation. *Journal of Neurophysiology*, *100*(5), 2549–2563. https://doi.org/10.1152/jn.90372.2008

Jones, D. K. (2008). Studying connections in the living human brain with diffusion MRI. *Cortex*, *44*(8), 936–952. https://doi.org/10.1016/j.cortex.2008.05.002

Kühn, A. A., & Volkmann, J. (2017). Innovations in deep brain stimulation methodology. *Movement Disorders*, *32*(1), 11–19. https://doi.org/10.1002/mds.26703

Lambert, C., Zrinzo, L., Nagy, Z., Lutti, A., Hariz, M., Foltynie, T., ... Frackowiak, R. (2012). Confirmation of functional zones within the human subthalamic nucleus: Patterns of connectivity and sub-parcellation using diffusion weighted imaging. *NeuroImage*, *60*(1), 83–94. https://doi.org/10.1016/j.neuroimage.2011.11.082

McIntyre, C. C., Grill, W. M., Sherman, D. L., & Thakor, N. V. (2004). Cellular effects of deep brain stimulation: Model-based analysis of activation and inhibition. *Journal of Neurophysiology*, *91*(4), 1457–1469. https://doi.org/10.1152/jn.00989.2003

McIntyre, C. C., & Hahn, P. J. (2010). Network perspectives on the mechanisms of deep brain stimulation. *Neurobiology of Disease*, *38*(3), 329–337. https://doi.org/10.1016/j.nbd.2009.09.022

Mehanna, R., & Jankovic, J. (2013). Movement disorders in cerebrovascular disease. *The Lancet Neurology*, *12*(6), 597–608. https://doi.org/10.1016/S1474-4422(13)70057-7

Mehanna, R., & Lai, E. C. (2013). Deep brain stimulation in Parkinson's disease. *Translational Neurodegeneration*, *2*(1), 22. https://doi.org/10.1186/2047-9158-2-22

Miocinovic, S., Somayajula, S., Chitnis, S., & Vitek, J. L. (2013). History, applications, and mechanisms of deep brain stimulation. *JAMA Neurology*, *70*(2), 163–171. https://doi.org/10.1001/2013.jamaneurol.45

Nambu, A., Tokuno, H., & Takada, M. (2002). Functional significance of the cortico-subthalamo-pallidal "hyperdirect" pathway. *Neuroscience Research*, *43*(2), 111–117. https://doi.org/10.1016/S0168-0102(02)00027-5

Odekerken, V. J., van Laar, T., Staal, M. J., Mosch, A., Hoffmann, C. F., Nijssen, P. C., ... Mink, M. S. (2013). Subthalamic nucleus versus globus pallidus bilateral deep brain stimulation for advanced Parkinson's disease (NSTAPS study): A randomised controlled trial. *The Lancet Neurology*, *12*(1), 37–44. https://doi.org/10.1016/S1474-4422(12)70264-8

Petersen, M. V., Husch, A., Parsons, C. E., Lund, T. E., Sunde, N., & Østergaard, K. (2018). Using automated electrode localization to guide stimulation management in DBS. *Annals of Clinical and Translational Neurology*, *5*(7), 888–894. https://doi.org/10.1002/acn3.589

Plantinga, B. R., Temel, Y., Duchin, Y., Uludağ, K., Patriat, R., Roebroeck, A., … Harel, N. (2018). Individualized parcellation of the subthalamic nucleus in patients with Parkinson's disease with 7T MRI. *NeuroImage*, *168*, 403–411. https://doi.org/10.1016/j.neuroimage.2016.09.023

Pollo, C., Kaelin-Lang, A., Oertel, M. F., Stieglitz, L., Taub, E., Fuhr, P., … Schüpbach, M. (2014). Directional deep brain stimulation: An intraoperative double-blind pilot study. *Brain*, *137*(7), 2015–2026. https://doi.org/10.1093/brain/awu102

Riva-Posse, P., Choi, K. S., Holtzheimer, P. E., Crowell, A. L., Garlow, S. J., Rajendra, J. K., … Mayberg, H. S. (2018). A connectomic approach for subcallosal cingulate deep brain stimulation surgery: Prospective targeting in treatment-resistant depression. *Molecular Psychiatry*, *23* (4), 843. https://doi.org/10.1038/mp.2017.59

Sun, H., Chen, Y., Huang, Q., Lui, S., Huang, X., Shi, Y., … Gong, Q. (2017). Psychoradiologic utility of MR imaging for diagnosis of attention deficit hyperactivity disorder: A radiomics analysis. *Radiology*, *287*(2), 620–630. https://doi.org/10.1148/radiol.2017170226

Svetnik, V., Liaw, A., Tong, C., Culberson, J. C., Sheridan, R. P., & Feuston, B. P. (2003). Random forest: A classification and regression tool for compound classification and QSAR modeling. *Journal of Chemical Information and Computer Sciences*, *43*(6), 1947–1958. https://doi.org/10.1021/ci034160g

Toda, H., Sawamoto, N., Hanakawa, T., Saiki, H., Matsumoto, S., Okumura, R., … Hashimoto, N. (2009). A novel composite targeting method using high-field magnetic resonance imaging for subthalamic nucleus deep brain stimulation. *Journal of Neurosurgery*, *111*(4), 737–745. https://doi.org/10.3171/2008.12.JNS0861

Vanegas-Arroyave, N., Lauro, P. M., Huang, L., Hallett, M., Horovitz, S. G., Zaghloul, K. A., & Lungu, C. (2016). Tractography patterns of subthalamic nucleus deep brain stimulation. *Brain*, *139*(4), 1200–1210. https://doi.org/10.1093/brain/aww020

Volkmann, J., Herzog, J., Kopper, F., & Deuschl, G. (2002). Introduction to the programming of deep brain stimulators. *Movement Disorders: Official Journal of the Movement Disorder Society*, *17*(S3), S181–S187. https://doi.org/10.1002/mds.10162

Volkmann, J., Moro, E., & Pahwa, R. (2006). Basic algorithms for the programming of deep brain stimulation in Parkinson's disease. *Movement Disorders: Official Journal of the Movement Disorder Society*, *21*(S14), S284–S289. https://doi.org/10.1002/mds.20961

Shukla, A. W., & Okun, M. S. (2014). Surgical treatment of Parkinson's disease: Patients, targets, devices, and approaches. *Neurotherapeutics*, *11* (1), 47–59. https://doi.org/10.1007/s13311-013-0235-0

Williams, D., Tijssen, M., van Bruggen, G., Bosch, A., Insola, A., Di Lazzaro, V., … Brown, P. (2002). Dopamine-dependent changes in the functional connectivity between basal ganglia and cerebral cortex in humans. *Brain*, *125*(7), 1558–1569. https://doi.org/10.1093/brain/awf156

Wodarg, F., Herzog, J., Reese, R., Falk, D., Pinsker, M. O., Steigerwald, F., … Volkmann, J. (2012). Stimulation site within the MRI–defined STN predicts postoperative motor outcome. *Movement Disorders*, *27*(7), 874–879. https://doi.org/10.1002/mds.25006

Zhang, D., Lin, H., Liu, J., Liu, Z., Yan, J., & Cai, X. (2019). Electrode reconstruction assists postoperative contact selection in deep brain stimulation. *World Neurosurgery*, *125*, e442–e447. https://doi.org/10.1016/j.wneu.2019.01.101

## SUPPORTING INFORMATION

Additional supporting information may be found online in the Supporting Information section at the end of this article.

---

**How to cite this article:** Lin H, Na P, Zhang D, Liu J, Cai X, Li W. Brain connectivity markers for the identification of effective contacts in subthalamic nucleus deep brain stimulation. *Hum Brain Mapp*. 2020;41:2028–2036. https://doi.org/10.1002/hbm.24927